J Mater Sci (2020) 55:738–747

Materials for life sciences

Drug self-gating fluorescent nanoparticles for pH-responsive doxorubicin delivery

Guoling Li[1,*], Bo Yang[1], and Chuantao Gu[1]

[1] College of Materials Science and Engineering, Qingdao University, Qingdao 266071, China

Received: 28 June 2019
Accepted: 10 September 2019
Published online: 10 October 2019

ABSTRACT

Intelligent drug delivery systems have attracted great attention in the field of biomedicine and cancer diagnosis. In this work, a drug delivery system that can be gated by doxorubicin itself and together with pH-responsive ability has been designed and prepared based on the upconversion nanoparticles. The drug delivery system is a special core–shell structure, consisting of upconversion nanoparticle core and mesoporous silica shell. The new system tactfully bypasses the use of auxiliary capping agents and exhibits desirable drug release at pH = 5, enhancing HeLa cells inhibition. The introduction of Schiff base plays a key role in the process of achieving pH-responsive drug release. Moreover, upconversion nanoparticles could emit bright yellow-green fluorescence (540 nm) under the irradiation of near-infrared light (980 nm) for in vivo bioimaging. This characteristic provides the possibility of locating tumor tissues and real-time tracing drug delivery.

Introduction

Research on cancer is still a crucial issue worldwide; precise diagnosis and fundamental therapy of cancer are still important challenges. Stimuli-responsive drug delivery systems that could specifically transport antineoplastic drugs into tumor tissues with minimal premature release are highly expected [1, 2]. In this respect, nanostructured materials perform a very important role because of their intrinsic small size that allows their easy incorporation as probes into living cells or organisms [3, 4]. Multifunctional response nanocomposites for stimuli-responsive drug delivery have been developed, such as pH, temperature, light, ionic strength and magnetic field [5–9].

Among the various multifunctional nanoparticles, due to the special characteristics of tunable multicolor sharp emission, large anti-Stokes shifts, great photostability, superior light penetration depth and autofluorescence-free nature, rare-earth-doped upconversion nanoparticles (UCNPs) have been demonstrated as one of the most promising biomedicine nanomaterials [10–13]. In the field of biomedicine, UCNPs can be used as drug carriers and luminescence labels to track the drug release process in living system [14–17]. However, the poor biocompatibility and low specific surface area of UCNP nanoparticles restrict their direct applications [18, 19].

Address correspondence to E-mail: liguoling@qdu.edu.cn

https://doi.org/10.1007/s10853-019-04020-7

Mesoporous silica nanomaterial (MSN) is an outstanding drug carrier with excellent biocompatibility and the ease of surface modification [20, 21]. UCNPs composites with MSN as drug loading materials have attracted considerable attention [22]. To realize the stimuli-responsiveness, organic polymer molecules [23], DNA [24], peptides [25] and inorganic nanoparticles [26] have been usually used as capping agents coated outside the UCNP@MSN composites. Jun Lin et al. reported a controlled release system based on upconversion luminescent microspheres of $NaYF_4$:Yb/Er@SiO_2 coated with the smart hydrogel poly (N-isopropylacrylamide-co-methacrylic acid) shell [27]. Boshi Tian et al. prepared the functional UCNPs@mSiO_2-PAA nanocomposite with UCNPs as core and poly (acrylic acid) (PAA)-gated mesoporous silica as shell for oral drug delivery [23]. A facile methodology UCNPs@mSiO_2-PEG was developed to construct as a multifunctional anticancer drug nanocarrier by combining the special advantages of upconversion nanoparticles and mesoporous silica, which can be used as an anticancer drug doxorubicin (DOX) delivery carrier and applied for magnetic resonance imaging (MRI) imaging [28]. Drug delivery system with the features of multifunctional synergy has become a hot research topic. Despite the excellent performance, the delivery systems still have critical problems such as unpredictable toxicity of the capping agents as well as the scarcity of bioresponsiveness [29, 30].

In the present study, a drug delivery system that can be gated by DOX itself and together with pH-responsive ability has been designed and prepared based on the upconversion nanoparticles (UCNPs), shown in Fig. 1a. MSN was used as the intermediate layer covered on the UCNPs for loading with doxorubicin DOX. The drug DOX itself could act as a pH-sensitive "gatekeeper" to minimize the potential risks of auxiliary capping agents. This system has dual functions with responsive drug delivery and fluorescence imaging. The fluorescence property of UCNPs provides the possibility of locating tumor tissues and real-time tracing drug delivery.

Experimental

Preparation of UCNP@nSiO_2@mSiO_2 nanoparticles

According to the literature protocols with modifications, UCNPs were synthesized via hydrothermal reaction. In a typical experiment, $YCl_3{\cdot}6H_2O$ (0.78 mmol), $YbCl_3{\cdot}6H_2O$ (0.2 mmol) and $ErCl_3{\cdot}6H_2O$ (0.02 mmol) were added to a three-neck round-bottom flask containing 15 ml H_2O. Then, 15 ml of disodium EDTA solution (1 mmol) and 15 ml of NaF solution (6 mmol) were sequentially added with magnetic stirring. After stirring for 1 h, the mixture was transferred to a Teflon autoclave, and the reaction was heated at 180 °C for 2 h. After the temperature was cooled to room temperature, the white precipitate was collected by centrifugation, washed with water and ethanol, and finally dried in a vacuum oven.

The as-prepared UCNPs were coated with dense silica and mesoporous silica sequentially by means of modified sol–gel reaction. Firstly, a quantity of UCNPs was dispersed into a mixture consisting of 1 ml ammonia, 15 ml distilled water and 60 ml ethanol, and then, 50 µl TEOS was slowly add. After hydrolysis reaction at room temperature for 4 h, the UCNP@nSiO_2 nanoparticles were collected by centrifugation and washed. Afterward, the above coating process was repeated to get UCNP@nSiO_2@C-SiO_2 except that CTAB should be added as pore template and the amount of TEOS was increased to 100 µl.

Surface functionalization of UCNP@nSiO_2@mSiO_2

An amount of UCNP@nSiO_2@C-SiO_2 nanoparticles were dispersed in 30 ml toluene containing 50 µl APTES and 10 µl TEA. After the solution was uniformly dispersed by ultrasound, the reaction was refluxed at 110 °C oil bath for 12 h under the protection of argon, receiving UCNP@nSiO_2@C-SiO_2-NH_2. The product was collected by centrifugation and washed with toluene and ethanol several times.

In order to modify the external surface with aldehyde groups, the UCNP@nSiO_2@C-SiO_2-NH_2 was put into 30 ml deionized water/DMSO mixture solution (4:1, v/v), containing 4-formylbenzoic acid (15.0 mg, 0.10 mmol), EDC (23.0 mg, 0.12 mmol) and NHS (13.8 mg, 0.12 mmol). After stirring at room temperature for 24 h, aldehyde groups were successfully introduced onto the surface by amidation reaction between carboxyl groups and amino groups for subsequent drug delivery. Finally, the nanoparticles were dispersed in 100 ml acetone and refluxed at 80 °C overnight to remove the surfactant template.

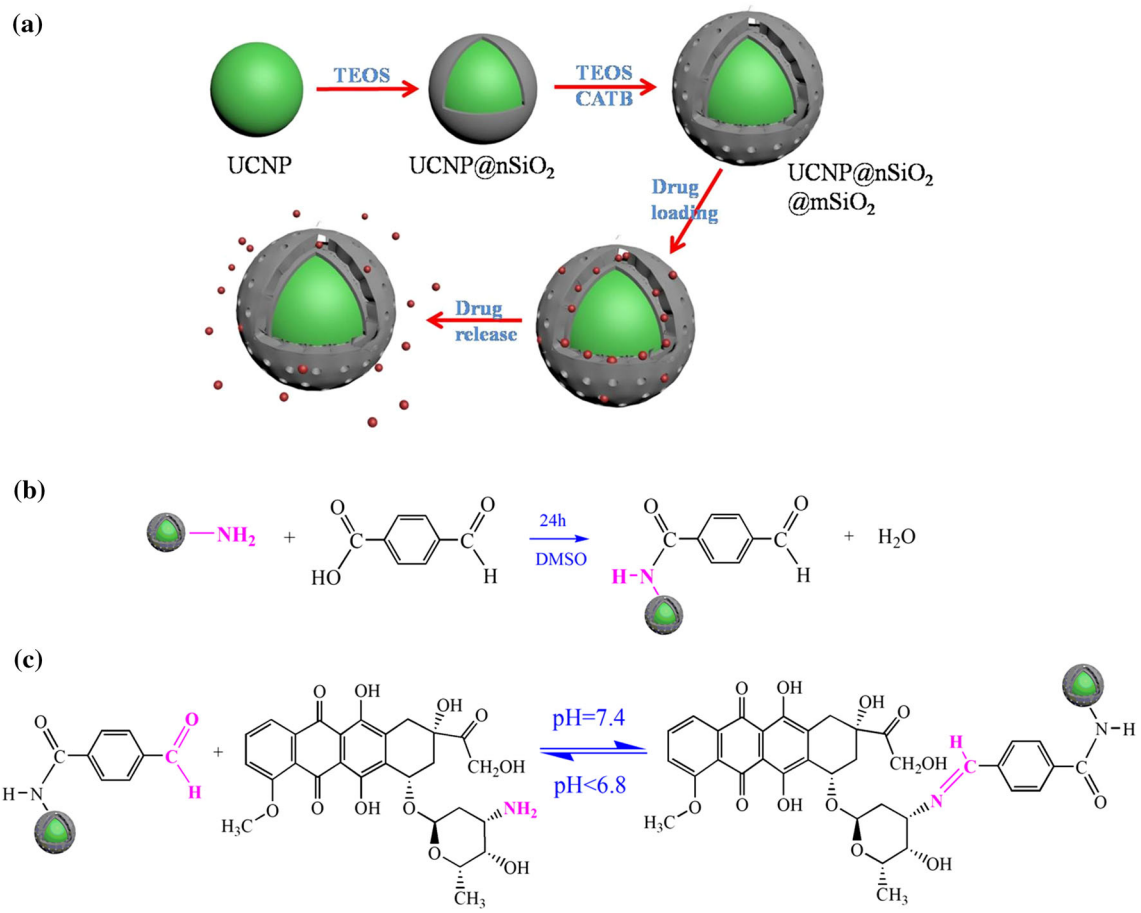

Figure 1 Schematic of the UCNP-based drug delivery system.

In this way, the UCNP@nSiO$_2$@mSiO$_2$-CHO nanoparticle was obtained, as shown in Fig. 1b.

Drug loading and release

DOX was chosen as a model drug to investigate the drug delivery behavior from the UCNP@nSiO$_2$@-mSiO$_2$-CHO nanocomposite. UCNP@nSiO$_2$@mSiO$_2$-CHO (10 mg) was soaked in 10 mL deionized water containing 50 μg DOX at pH 6.0 and room temperature for 24 h in the dark. Adjusting the solution to pH = 8.0 and stirring for 2 h, the outlets of mesoporous nanoparticles were capped with DOX through reversible covalent benzoic–imine linkage between the aldehyde group and amine group in DOX. After centrifugation and washing, the DOX-loaded and DOX-gated nanoparticles were prepared. The schematic diagram is shown in Fig. 1c.

To study the pH-responsive release properties, the DOX loading samples were immersed in 10 mL of pH = 7.4, 6.8 and 5.0 PBS buffer solutions at room temperature with gentle shaking. The amounts of released DOX were analyzed by UV–vis spectrophotometer. The details are in the support information.

In vitro cytotoxicity assay

The in vitro cytotoxicity was measured by MTT assay on HeLa cells. Cells with a density of 20000 cells per well were cultured in a 96-well plate at 37 °C for 24 h. Then, the cells were incubated with different concentrations of UCNP@n-SiO$_2$@mSiO$_2$, DOX self-gated nanoparticles and free UCNP for 24 h. Then, after cleaning with PBS, 5.0 mg MTT (20μl of 3-(4, 5-dimethyl-2-thiazolyl)-2, 5-diphenyl-2-H-tetrazolium bromide solution) was added to 96-well plates. After 4 h, the solution was removed and cleaned, and then, 100 μl of dimethyl sulfoxide (DMSO) was added to each well and shaken slowly for 10 min at room temperature.

Characterization

Transmission electron microscopy (TEM) was performed on JEM-2100F to characterize the change of sample morphology. The crystal structures were characterized by X-ray diffraction (XRD, Rigaku D/max 200 diffractometer, Cu Kα) at a scan rate of 2°/min. Nitrogen adsorption–desorption isotherm was measured on a COULTER SA 3100 apparatus at a liquid nitrogen temperature (77 K). The surface modification and functional group modification of the material can be tested by Fourier transformation infrared spectrometer (FT-IR). IVIS Lumina XRMS series III (PerkinElmer) was used for the in vivo imaging. The UC emission spectra were obtained on an FLS1000 Edinburgh Analytical Instrument equipped using a 980 nm laser as the excitation source.

Results and discussion

Preparation and characterization of UCNP@nSiO$_2$@mSiO$_2$ nanoparticles

UCNPs were synthesized using modified hydrothermal method. The morphology and structures of samples were tested by TEM. In Fig. 2a, it can be observed that the $NaFY_4$:Yb, Er nanocrystals are well monodispersed in water and display uniform morphology with a size of around 100 nm. In the silica coating process, for no fluorescence quenching of the nanoparticles, a thin and dense silica layer was first coated on the surface of UCNPs. Figure 2b shows the UCNP@nSiO$_2$ nanoparticles; the thickness of solid silica is about 8 nm. The resulting particles were then coated with a layer of mesoporous silica; Fig. 2c shows the UCNP@nSiO$_2$@mSiO$_2$ structure. Due to the different electron penetrability between the core and shell, it is obvious that there are two layers coated on the core and the thickness of mesoporous silica is about 22 nm. Except for a slight aggregation, the similar morphological feature of pure UCNPs was kept.

The XRD patterns of the UCNPs, UCNP@nSiO$_2$ and UCNP@nSiO$_2$ @mSiO$_2$ are separately displayed in Fig. 3. Compared with the cubic phase of β-NaYF4 (JCPDS: 06-0342), they all show face-centered cubic phase structures, suggesting that the samples possess intact crystal structure. In the patterns of UCNPs@nSiO$_2$@mSiO$_2$, the peak at $2\theta = 22°$ is a broad diffraction peak of amorphous silica, which suggests that the mesoporous silica shell was coated on the UCNPs surface.

Figure 4 shows the N_2 adsorption–desorption isotherms of UCNPs@nSiO$_2$@mSiO$_2$ nanocomposites. The sample exhibits typical type-IV isotherms, which further confirms the existence of mesoporous structure. The BET surface area and total pore volume of UCNPs@@nSiO$_2$@mSiO$_2$ were 88.76 $m^2\ g^{-1}$ and 0.096 $cm^3\ g^{-1}$, respectively. The BJH pore sizes of UCNPs@nSiO$_2$@mSiO$_2$ were estimated to be 4.3 nm. Large specific surface area and moderate pore size provide satisfactory preconditions for the loading of drugs.

The upconversion luminescence spectra and the following photographs of UCNPs, UCNPs@nSiO$_2$ and UCNPs@nSiO$_2$@mSiO$_2$ under 980-nm excitation are shown in Fig. 5. It can be seen from the graph that when excited by 980 nm laser, all samples emit bright yellow-green fluorescence, and the fluorescence spectra show obvious two emission peaks at 540 nm and 655 nm, resulting in the energy transition from $^4S_{3/2} \rightarrow {}^4I_{15/2}$ and $^4F_{9/2} \rightarrow {}^4I_{15/2}$ of Er^{3+} ions, respectively. The intensity of emission peaks

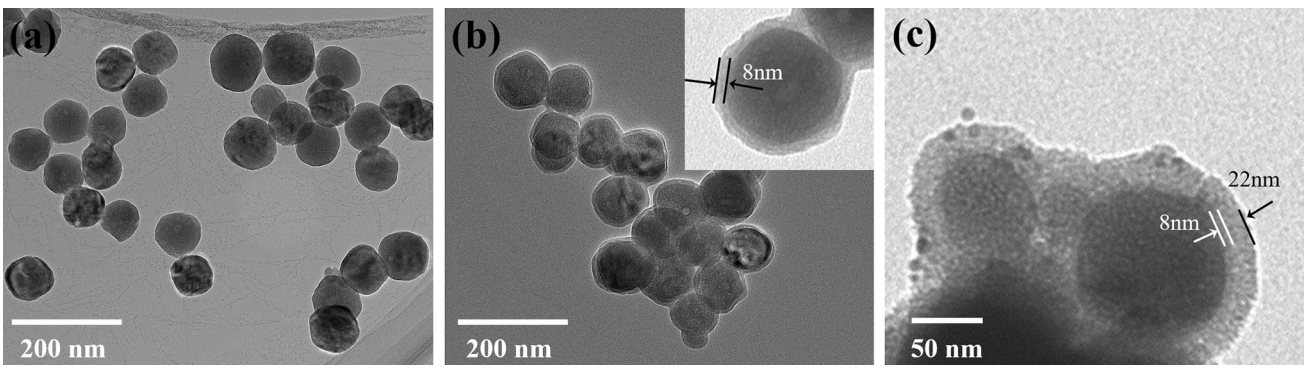

Figure 2 TEM images of **a** UCNPs, **b** UCNP@nSiO$_2$ and **c** UCNP@nSiO$_2$@mSiO$_2$.

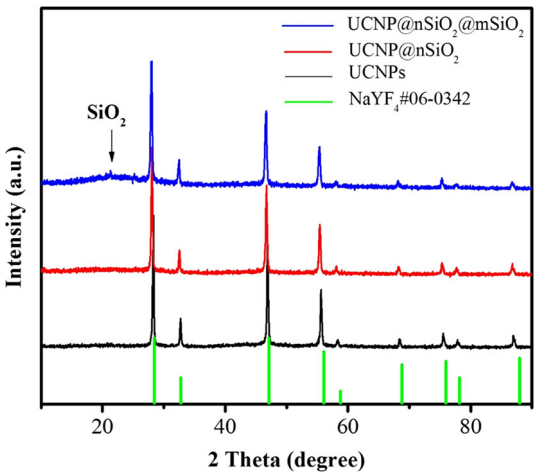

Figure 3 XRD patterns of UCNPs, UCNP@$nSiO_2$, UCNPs@$nSiO_2$@$mSiO_2$ and the standard card of β-NaYF4 (JCPDS: 06-0342).

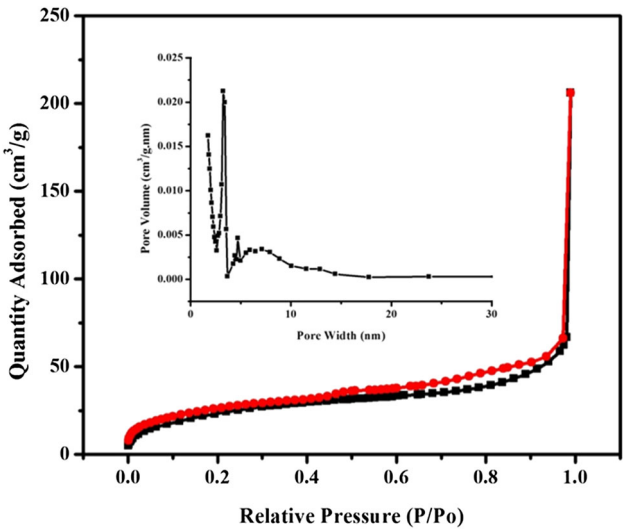

Figure 4 N_2 adsorption–desorption isotherm and pore size distribution (inset) of UCNP@$nSiO_2$@$mSiO_2$ nanoparticles.

decreases to a certain extent after coated with SiO_2 shell layer by layer on the particle surface, but still retains strong yellow-green emission intensity.

Surface functionalization and characterization of UCNP@$nSiO_2$@$mSiO_2$

Schiff base reaction is a reversible condensation reaction sensitive to acid and base. The formed imine group is very active and can be broken in acidic environment. Amino groups can be first grafted onto UCNP@$nSiO_2$@$mSiO_2$ surface with silane coupling

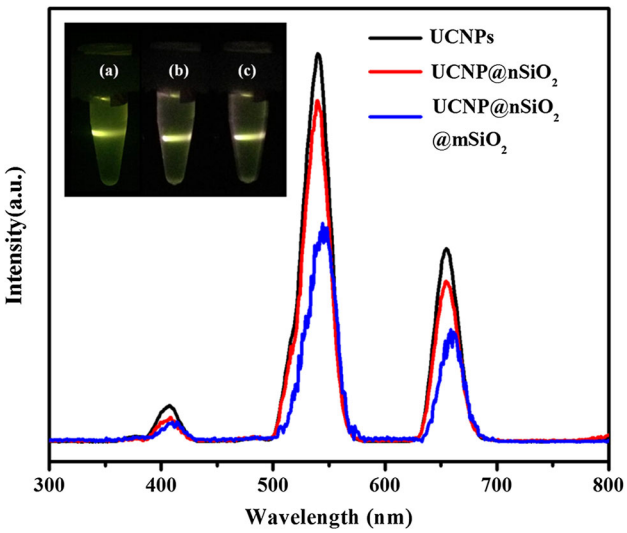

Figure 5 Fluorescence spectra and digital photographs of (a) UCNPs, (b) UCNP@$nSiO_2$ and (c) UCNP@$nSiO_2$@$mSiO_2$.

agent APTES. Then, 4-carboxybenzaldehyde is introduced onto the surface of particles to complete the aldehyde modification. Schiff base reaction between amino groups inherent in DOX and aldehyde groups on nanoparticles comes to achieve DOX self-capped mesoporous and pH-responsive drug release.

Figure 6a shows the chromogenic reaction of ninhydrin; the UCNP@$nSiO_2$@$mSiO_2$-NH_2 solution turned blue, while the supernatant does not change in color. The comparison results show that amino groups have been successfully grafted onto the surface of the particles without the existence of free APTES. Figure 6b displays the FT-IR spectra of UCNP@$nSiO_2$@$mSiO_2$, UCNP@$nSiO_2$@$mSiO_2$-NH_2 and UCNP@$nSiO_2$@$mSiO_2$-CHO. For UCNP@n SiO_2@$mSiO_2$ FT-IR spectroscopy, absorption bands at 1080 cm^{-1} (Si–O–Si antisymmetric stretching vibration), 800 cm^{-1} (Si–O–Si symmetric stretching vibration) and 960 cm^{-1}(Si–OH bending vibration) are presented. After modification with APTES, the stretching vibration of C–N and N–H increases the peak at 1030–1230 cm^{-1} and 3400–3500 cm^{-1}, which is shown in curve (II). For the UCNP@$nSiO_2$@$mSiO_2$-CHO shown in curve (III), the characteristics of amide bond (1643 cm^{-1}) and aldehyde group (1551 cm^{-1}) were clearly observed, confirming that UCNP@$nSiO_2$@$mSiO_2$ was functionalized successfully with –CHO groups.

Nanocomposites modified with –CHO groups have high fluorescence properties, as shown in

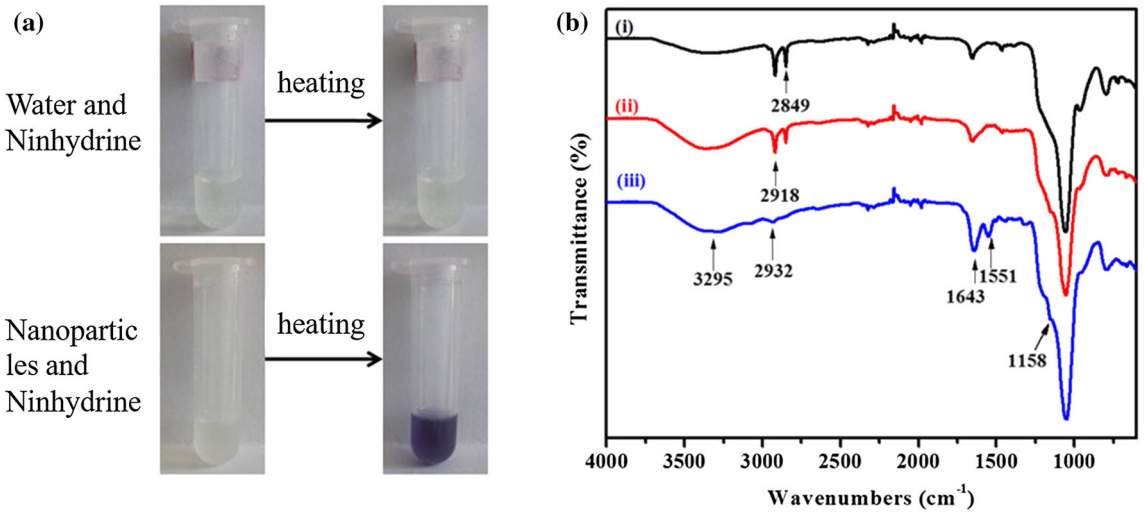

Figure 6 **a** Chromogenic reaction of ninhydrin, **b** FT-IR spectra of (i) UCNP@nSiO$_2$@mSiO$_2$, (ii) UCNP@nSiO$_2$@mSiO$_2$–NH$_2$, (iii) UCNP@nSiO$_2$@mSiO$_2$-CHO.

Fig. 7A. Figure 7B displays the in vivo fluorescence images of UCNPs@nSiO$_2$@mSiO$_2$-CHO after intravenous injection into the mice through a tail vein. Under 980-nm excitation, clear fluorescence signals in the mice were detected after 2 h of injection. Over time, the fluorescence of mice tail gradually weakened, and fluorescence signals appeared in the left kidney, indicating that the particles gradually entered the kidney with blood circulation. High fluorescence intensity was detected in the urine and urethra, as shown in Fig. 5B-d, which means UCNPs@nSiO$_2$@mSiO$_2$-CHO nanoparticles exhibit good biocompatibility and can be excreted in urine. The in vivo results confirm the high luminous efficiency and low systematic toxicity of the self-gated nanoparticles.

Drug loading and release

To determine the gating effect of DOX, we further explore the drug delivery capacity of UCNP@nSiO$_2$@mSiO$_2$-CHO. The amount of DOX in the nanocarrier solution can be determined by the characteristic DOX absorption peak at 500 nm. Figure 8a shows the loading profile of composite nanoparticles under different DOX initial concentrations. With the concentration increasing, the drug adsorption capacity of the carrier increases gradually. When the initial concentration increases above 60 μg/ml, the adsorption capacity of the carrier reaches saturation, up to 20 μg/mg or more, which is higher than UCNP@nSiO$_2$@mSiO$_2$ without any functional treatment (Fig. S2). This phenomenon

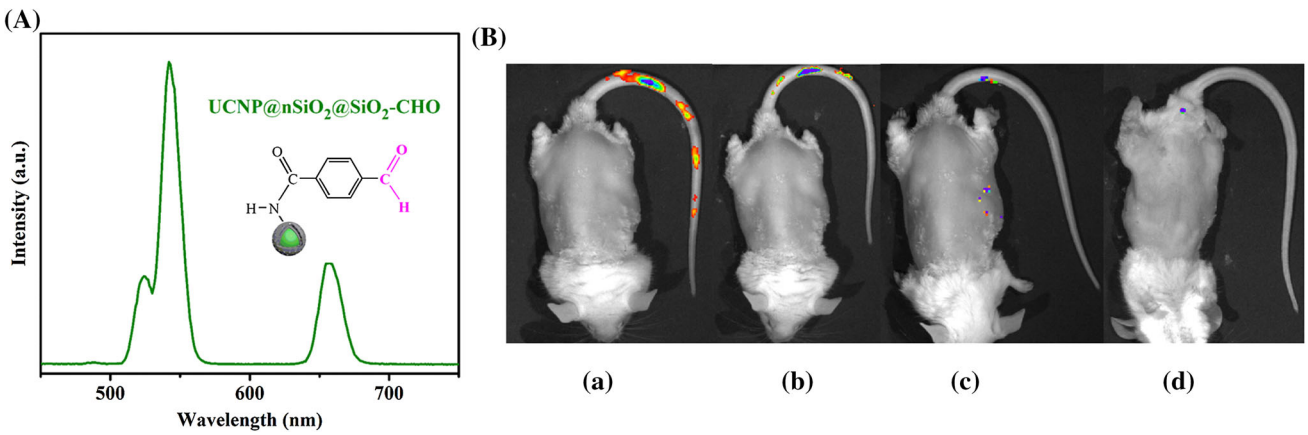

Figure 7 **A** Fluorescence spectra of UCNP@nSiO$_2$@mSiO$_2$-CHO, **B** in vivo fluorescence images of injection after (a) 2 h, (b) 24 h, (c) 72 h, (d) 86 h.

attributes to the capillary action and van der Waals force of porous structure of the composite nanoparticles. The capillary action of pore and van der Waals force make the drug to be easily loaded, and with the increase in loading, the action force gradually decreases, thus reaching the saturated adsorption of the drug. Then, the covalent benzoic–imine linkage achieves the capping effect in alkaline condition.

Figure 8b displays the DOX release profiles in PBS buffer solution with different pH values. Obviously, the DOX release behavior exhibits a significantly pH-dependent property. In alkaline and neutral buffer (pH = 7.4, 6.8), the release rate of drug in the carrier is extremely low, and the cumulative release of DOX is only about 17%, which displays the excellent DOX self-gating effect under physiological conditions. In contrast, under acidic environment (PH = 5), large amount of DOX (~ 45.5%) release is observed over the same time period. However, there is no pH response for drug release process of single UCNP@nSiO2@mSiO$_2$, and the release rate is very high (Fig. S3). Clearly, in this work, the pH-controlled drug release system has been successfully constructed. The gatekeeper pH-responsive Schiff base reaction plays the vital role of controlled release of DOX. Under alkaline condition, the covalent benzoic–imine bond between DOX and –CHO groups seals the pore entrances of nanoparticles, causing the DOX molecules encapsulated in the blocked pore channels. A few release of DOX may be due to the adsorption of DOX on the external surface of UCNP@nSiO$_2$@mSiO$_2$-CHO. Under acidic environment, inverse reaction takes place and the covalent benzoic–imine bond is broken, resulting that the pore entrance is opened. These results demonstrate that without any auxiliary capping agents, the DOX-gated method in this study is a feasible strategy that meets the requirements of drug loading and achieves pH-responsive drug release, exhibiting its potential applicability in combination therapy.

Cytotoxicity

Cytotoxicity of the synthesized nanocomposite is evaluated by 3-[4,5-dimethylthiazol-2-yl]-2,5-diphenyltetrazolium bromide (MTT) assay on HeLa cells. From Fig. 9, after incubation with UCNP and

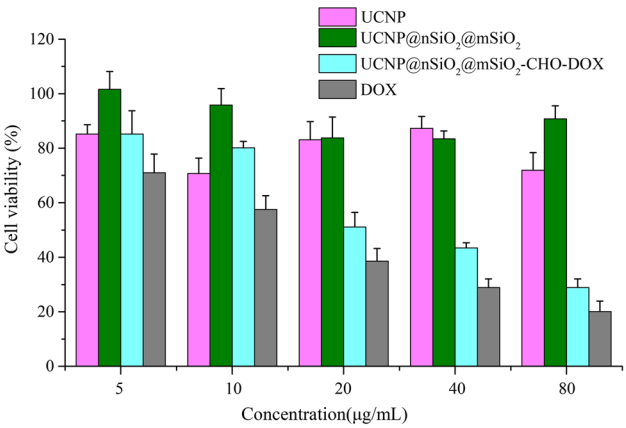

Figure 9 In vitro cell viability assay of UCNP, UCNP@nSiO$_2$@mSiO$_2$-CHO, UCNP@nSiO$_2$@mSiO$_2$-CHO-DOX and free DOX.

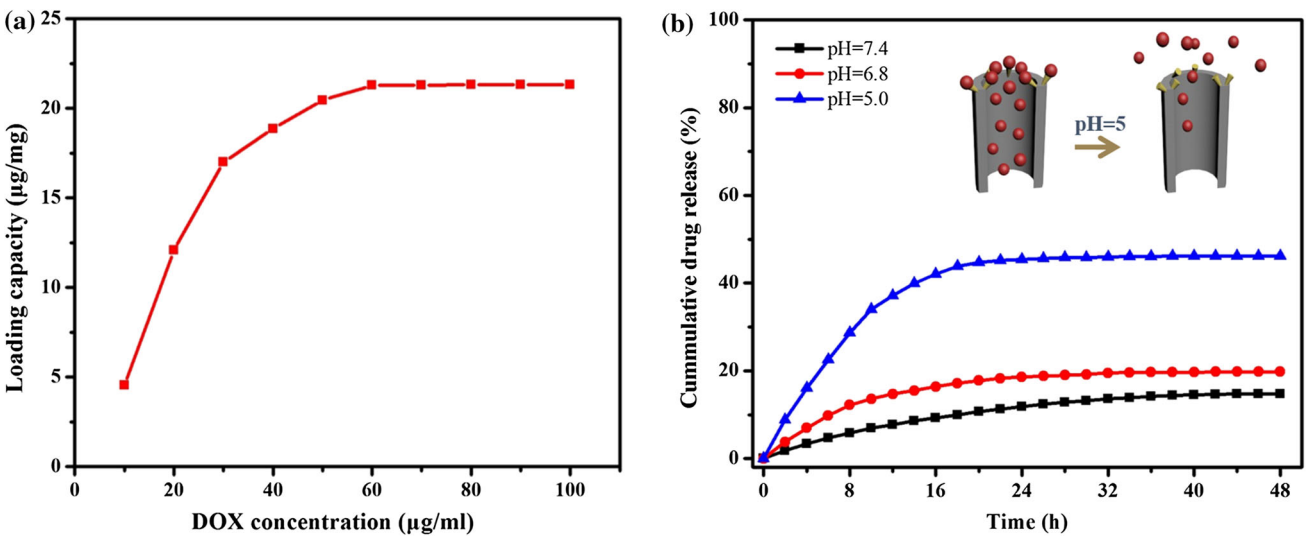

Figure 8 **a** DOX loading capacity of as-prepared UCNP@nSiO$_2$@mSiO$_2$-CHO; **b** DOX release at different pH conditions.

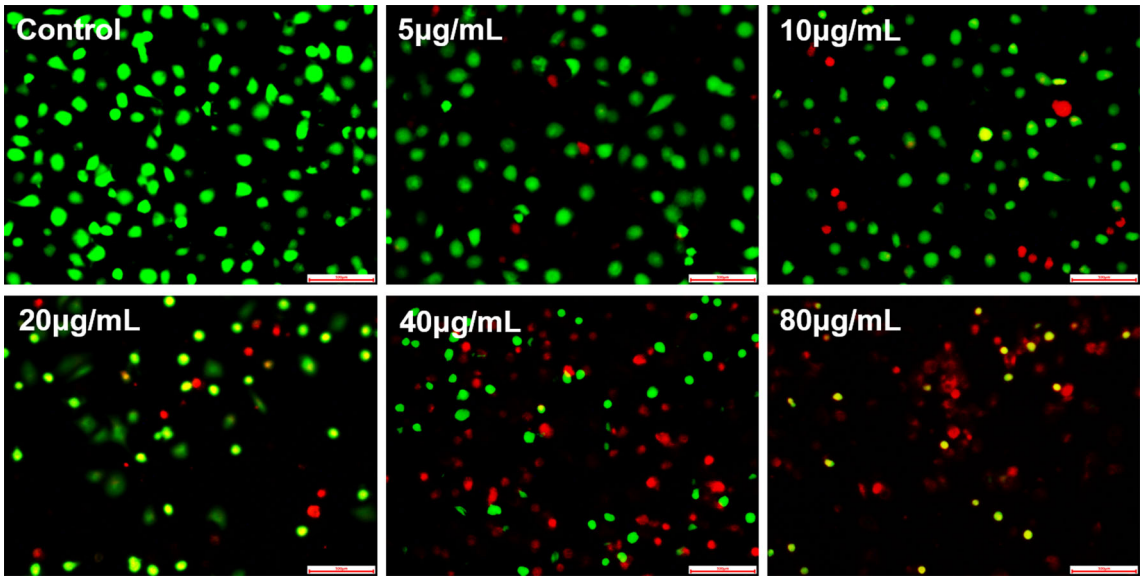

Figure 10 In vitro cytotoxicity against HeLa cells of UCNP@nSiO$_2$@mSiO$_2$-CHO-DOX to cells.

UCNP@nSiO$_2$@mSiO$_2$ nanoparticles with various concentrations of 0–80 μg/mL for 24 h, the cellular survival rate descended slightly with the increased concentration, especially cells with UCNP@nSiO$_2$@-mSiO$_2$, and the cellular viability was still higher than 90.72%, which implied that the samples exhibit a negligible cytotoxicity. The cells incubated with UCNP@nSiO$_2$@mSiO$_2$ exhibited a relative high survival rate, which indicated that SiO$_2$ coating modification can improve the biocompatibility of the nanocomposite. The prepared composite fluorescent nanoparticles display wonderful biocompatibility and can be used as drug carrier in the biomedical fields.

Furthermore, the cytotoxic effect of drug-loaded nanoparticles on HeLa cells was also investigated. Upon drug loading, the self-gated group UCNP@nSiO$_2$@mSiO$_2$-CHO-DOX could remarkably inhibit HeLa cell growth at a low concentration range. The cellular survival rate descended seriously with the increased concentration, displaying a similar concentration-dependent toxicity effect to the pure DOX. It mainly depends on the positive surface potential for cell internalization and subsequently the sustained DOX release from the pore channels of mesoporous nanocomposites. The cell viability assay for different times is shown in Fig. S4, a time-dependent toxicity can be observed for UCNP@nSiO$_2$@mSiO$_2$-CHO-DOX nanoparticles. Figure 10 shows the effect of UCNP@nSiO$_2$@mSiO$_2$-CHO-DOX on the apoptosis rate under different concentrations after 24 h. With the concentrations increasing, cell viability decreased rapidly. In the images of live cells (green) and dead cells (red), it is apparent that the tumor cells are almost totally killed when cultured with UCNP@nSiO$_2$@mSiO$_2$-CHO-DOX at 80 μg/mL after 24 h compared with the cells incubated with pure culture. Taken together, these results suggest the drug loading nanoparticles own the potential to selectively kill more cancerous cells than normal tissue/cells at weakly acidic tumor microenvironments.

Conclusion

We designed a multifunctional antitumor nanocarrier, which consists of facile drug self-gated, pH-sensitive and near-infrared fluorescence properties. Such a new pH-responsive system, gated by antitumor drug DOX itself, could tactfully bypass the use of complex capping agents. The pH-sensitive benzoic–imine covalent bond can effectively control the release of drugs. The new system, which exhibits desirable drug release at pH = 5, can effectively inhibit HeLa cells growth. More inspiringly, nanocomposites display distinctive autofluorescence characteristics because of rare-earth upconversion particles in the core. Excellent in vivo imaging data show that particles can be excreted with urine, reducing unpredictable medical risks. The autofluorescence characteristics also show general potential

for locating tumor tissues and real-time tracing drug delivery. The developed functional system provides promising applications in future cancer therapy by integrating cancer diagnosis and collaborative therapy.

Acknowledgements

Bo Yang and Guoling Li contributed equally in this work. This work is financially supported by National Natural Science Foundation of China (51804174), Natural Science Foundation of Shandong Province (ZR2017BEE010), and General Financial Grant from China Postdoctoral (2017M612203).

Electronic supplementary material: The online version of this article (https://doi.org/10.1007/s10853-019-04020-7) contains supplementary material, which is available to authorized users.

References

[1] Zelikin AN, Ehrhardt C, Healy AM (2016) Materials and methods for delivery of biological drugs. Nat Chem 8:997–1007

[2] Sun Q, Zhou Z, Qiu N, Shen Y (2017) Rational design of cancer nanomedicine: nanoproperty integration and synchronization. Adv Mater 29:16066281–160662818

[3] Juère E, Florek J, Bouchoucha M, Jambhrunkar S, Wong KY, Popat A, Kleitz F (2017) In vitro dissolution, cellular membrane permeability, and anti-inflammatory response of resveratrol-encapsulated mesoporous silica nanoparticles. Mol Pharm 14:4431–4441

[4] Pelaz B, Alexiou C, Alvarez-Puebla RA et al (2017) Diverse applications of nanomedicine. ACS Nano 11:2313–2381

[5] Ren D, Kratz F, Wang S (2014) Engineered drug-protein nanoparticle complexes for folate receptor targeting. Biochem Eng J 89:33–41

[6] Dai Z, Leung H, Lo P (2017) Stimuli-responsive self-assembled DNA nanomaterials for biomedical applications. Small 13:16028811-16

[7] Yang D, Yang G, Gai S, He F, Li C, Yang P (2017) Multifunctional theranostics for dual-modal photodynamic synergistic therapy via stepwise water splitting. ACS Appl Mater Interfaces 9:6829–6838

[8] Neubergera K, Boddupallia A, Bratlie KM (2018) Effects of arginine-based surface modifications of liposomes for drug delivery in Caco-2 colon carcinoma cells. Biochem Eng J 139:8–14

[9] Sun K, You C, Wang S et al (2018) NIR stimulus-responsive core–shell type nanoparticles based on photothermal conversion for enhanced antitumor efficacy through chemo-photothermal therapy. Nanotechnology 29:285302

[10] Du K, Xu X, Yao S, Lei P, Dong L, Zhang M, Feng J, Zhang H (2018) Enhanced upconversion luminescence and controllable phase/shape of NaYF4:Yb/Er crystals through Cu^{2+} ion doping. CrystEngComm 20:1945–1953

[11] Wang X, Xu J, Yang D, Sun C, Sun Q, He F, Gai S, Zhong C, Li C, Yang P (2018) Fe_3O_4@MIL-100(Fe)-UCNPs heterojunction photosensitizer: rational design and application in near infrared light mediated hypoxic tumor therapy. Chem Eng J 354:1141–1152

[12] Feng LL, Gai SL, He F, Dai YL, Zhong CN, Yang PP, Lin J (2017) Multifunctional mesoporous ZrO2 encapsulated upconversion nanoparticles for mild NIR light activated synergistic cancer therapy. Biomaterials 147:39–52

[13] Feng LL, He F, Liu B, Yang G, Gai SL, Yang PP, Li CX, Dai YL, Lv RC, Lin J (2016) g-C3N4 coated upconversion nanoparticles for 808 nm near-infrared light triggered phototherapy and multiple imaging. Chem Mater 28:7935–7946

[14] Feng LL, Wang CQ, Li CX, Gai SL, He F, Li RM, An GH, Zhong CN, Dai YL, Yang ZL, Yang PP (2018) Multifunctional theranostic nanoplatform based on Fe-mTa2O5@CuS-ZnPc/PCM for bimodal imaging and synergistically enhanced phototherapy. Inorg Chem 57:4864–4876

[15] Feng L, He F, Dai Y, Gai S, Zhong C, Li C, Yang P (2017) Multifunctional UCNPs@$MnSiO_3$@g-C_3N_4 nano-platform: improved ROS generation and reduced glutathione levels for highly efficient photodynamic therapy. Biomater Sci 5:2456–2467

[16] Chan M, Liu R (2017) Advanced sensing, imaging, and therapy nanoplatforms based on Nd^{3+}-doped nanoparticle composites exhibiting upconversion induced by 808 nm near-infrared light. Nanoscale 9:18153–18168

[17] Yang GX, Yang D, Yang PP, Lv RC, Li CX, Zhong CN, He F, Gai SL, Lin J (2015) A single 808 nm near-infrared light-mediated multiple imaging and photodynamic therapy based on titania coupled upconversion nanoparticles. Chem Mater 27:7957–7968

[18] Wang F, Qu X, Liu D, Ding C, Zhang C, Xian Y (2018) Upconversion nanoparticles-MoS_2 nanoassembly as a fluorescent turn-on probe for bioimaging of reactive oxygen species in living cells and zebrafish. Sens Actuators, B 274:180–187

[19] Xiao P, Ye S, Liao H, Wang D (2018) Magnetic-optical bifunctional properties of sub-20 nm beta-NaYF4:$Yb^{3(+)}$,

Er^{3+} @$NaGdF_4$ core-shell nanocrystals. J Alloys Compd 767:775–781

[20] Peruzynska M, Cendrowski K, Barylak M et al (2015) Study on size effect of the silica nanospheres with solid core and mesoporous shell on cellular uptake. Biomed Mater 10:065012

[21] Choi E, Kwak M, Jang B, Piao Y (2013) Highly monodisperse rattle-structured nanomaterials with gold nanorod core-mesoporous silica shell as drug delivery vehicles and nanoreactors. Nanoscale 5:151–154

[22] Jayakumar MKG, Bansal A, Li B, Zhang Y (2015) Mesoporous silica-coated upconversion nanocrystals for near infrared light-triggered control of gene expression in zebrafish. Nanomedicine 10:1051–1061

[23] Liu S, Tian B, Wu S, Wang Y, Huang J, Gao B, Wang Z (2018) pH-sensitive polymer-gated multifunctional upconversion NaYF4:Yb/Er@mSiO(2) nanocomposite for oral drug delivery. Microporous Mesoporous Mater 264:151–158

[24] Zhou L, Chen Z, Dong K, Yin M, Ren J, Qu X (2014) DNA-mediated construction of hollow upconversion nanoparticles for protein harvesting and near-infrared light triggered release. Adv Mater 26:2424–2430

[25] Bansal A, Gnanasammandhan MK, Zhang Y (2014) Multifunctional fluorescent upconversion nanocrystals for simultaneous imaging and delivery of peptide toxins. Mater Appl Sens Transducers III(605):364–367

[26] Lim W, Phua S, Xu H, Sreejith S, Zhao Y (2016) Recent advances in multifunctional silica-based hybrid nanocarriers for bioimaging and cancer therapy. Nanoscale 8:12510–12519

[27] Cheng Z, Chai R, Ma P, Dai Y, Kang X, Lian H (2013) Multiwalled carbon nanotubes and $NaYF_4$:Yb^{3+}/Er^{3+} nanoparticle-doped bilayer hydrogel for concurrent NIR-triggered drug release and up-conversion luminescence tagging. Langmuir 29:9573–9580

[28] Li C, Yang D, Ma P, Chen Y, Wu Y, Hou Z, Dai Y, Zhao J, Sui C, Lin J (2013) Multifunctional upconversion mesoporous silica nanostructures for dual modal imaging and in vivo drug delivery. Small 9:4150–4159

[29] Hamblin MR (2018) Upconversion in photodynamic therapy: plumbing the depths. Dalton Trans 47:8571–8580

[30] Gu B, Zhang QC (2018) Recent advances on functionalized upconversion nanoparticles for detection of small molecules and ions in biosystems. Adv Sci 5:17006091–170060916